Rechargeable membraneless glucose biobattery: Towards solid-state cathodes for implantable enzymatic devices

CrossMark

Alireza Ahmadian Yazdi [a], Roberto Preite [a], Ross D. Milton [b], David P. Hickey [b], Shelley D. Minteer [b], Jie Xu [a, *]

[a] Department of Mechanical and Industrial Engineering, University of Illinois at Chicago, Chicago, IL, 60607, USA
[b] Departments of Chemistry and Materials Science and Engineering, University of Utah, Salt Lake City, UT, 84112, USA

HIGHLIGHTS

- A rechargeable biobattery is made based on enzymatic catalysis of glucose oxidation.
- O_2-breathing electrode is replaced by solid-state Prussian Blue cathode.
- The biobattery can be utilized for *in vivo* power generation.
- The biobattery can effectively operate in a membraneless configuration.

ARTICLE INFO

ABSTRACT

Enzymatic biobatteries can be implanted in living organisms to exploit the chemical energy stored in physiological fluids. Generally, commonly-used electron donors (such as sugars) are ubiquitous in physiological environments, while electron acceptors such as oxygen are limited due to many factors including solubility, temperature, and pressure. The wide range of solid-state cathodes, however, may replace the need for oxygen breathing electrodes and serve in enzymatic biobatteries for implantable devices. Here, we have fabricated a glucose biobattery suitable for *in vivo* applications employing a glucose oxidase (GOx) anode coupled to a solid-state Prussian Blue (PB) thin-film cathode. PB is a non-toxic material and its electrochemistry enables fast regeneration if used in a secondary cell. This novel biobattery can effectively operate in a membraneless architecture as PB can reduce the peroxide produced by some oxidase enzymes. The resulting biobattery delivers a maximum power and current density of 44 μW cm^{-2} and 0.9 mA cm^{-2}, respectively, which is *ca.* 37% and 180% higher than an equivalent enzymatic fuel cell equipped with a bilirubin oxidase cathode. Moreover, the biobattery demonstrated a stable performance over 20 cycles of charging and discharging periods with only *ca.* 3% loss of operating voltage.

© 2017 Elsevier B.V. All rights reserved.

1. Introduction

Biofuel cells offer unique features in comparison to chemical fuel cells, such as the ability to operate at room temperature and near neutral pH, biocompatibility, ease of miniaturization, possessing a small environmental footprint and low-cost power production [1–3]. A biofuel cell consists of an anode and a cathode that are separated by a liquid electrolyte, often employing a membrane to regulate the transport of ions between the cathodic and anodic compartments. At the anode a biofuel (electron donor) is oxidized with the aid of biological catalysts such as enzymes or whole microbes. Electrons that are released *via* the oxidation of biomass pass through an external load to produce power and eventually combine at the cathode with protons to reduce an electron acceptor, such as oxygen. Typically, metal catalysts (such as platinum) or biomolecules (such as enzymes) are used to catalyze the cathodic reaction. Enzymatic fuel cells (EFCs) are devices that convert biofuels such as glucose [4,5], fructose [6,7], or alcohols [8], to electricity utilizing enzymatic catalysts at the anode and/or cathode. A wide range of redox enzymes have been used in EFCs providing options for many energy-related applications, such as low-power electronics [9], lab-on-a-chip devices [10], self-powered sensors [11],

and implantable energy harvesting units [12].

Although there are various limitations to the use of EFCs for *in vivo* power generation, these limitations are expected to be overcome in the near future due to a growing interest in utilizing EFCs for implantable biomedical devices. One reason is that most of the biocatalysts utilized in EFCs are evolved to efficiently catalyze the reactions at physiological temperature and pH, yielding products that are tolerable to the complex host environment [12]. Due to the availability of biofuels (*i.e.*, glucose) in many living species and physiological fluids, glucose EFCs are promising units to harvest energy within living organisms for implantable devices. However, there are a number of hurdles that limit the applicability of the conventional design of EFCs in an *in vivo* environment. First of all, molecular oxygen (O_2) is the primary choice of electron acceptor due to its high standard reduction potential (~1.229 V *vs.* standard hydrogen electrode) in traditional designs. However, physiological O_2 concentrations are often low and constantly fluctuating (~0.1 mM) [12,13], leading to variations in performance and low current densities for EFCs. The use of air-breathing cathodes could be considered as a solution for such limitations, although they should be assembled in subcutaneous devices (limiting the range of applications) and may impose extra challenges in their design. Secondly, most EFC cathodes utilizing O_2-reducing enzymes are single-use, where enzymatic activity diminishes over time.

Prussian Blue (PB) or ferric ferrocyanide ($Fe_4^{III}[Fe_2^{II}(CN)_6]_3$) belongs to a family of materials known as transition metal hexacyanides with a general chemical formula of $A_xPR(CN)_6$ where A is an alkali cation and P and R are iron (Fe) atoms for the most common type of PB [14]. The cubic face-centered structure of the PB crystal with wide channels allows for the rapid intercalation of metal ions and protons (Fig. 1). Therefore, PB and its analogous have been extensively explored as cathodic materials for monovalent [15–18] and multivalent [6,19–22] metal-ion batteries. Moreover, PB has long served as a reliable catalyst for biosensor applications [23–25]. For example, Sekretaryova et al. [25] introduced a self-powered cholesterol biosensor that utilized PB alongside immobilized cholesterol oxidase (ChOx), whereby H_2O_2 (produced in proportion to cholesterol oxidation) is detected by PB. More recently, PB has been tested in biofuel cells and biobatteries. Yu et al. [26] introduced a novel integrated photoelectrochemical biofuel cell (PBFC) by taking advantage of the PB/Prussian White (PW) redox

couple for storage and conversion of solar energy and biomass into electricity. Addo et al. [27] reported the transition of an ethanol biofuel cell towards a rechargeable biobattery, utilizing NAD-dependent alcohol dehydrogenase (ADH) as the anodic catalyst immersed in butyl-3-methylimidazolium chloride (BMIMCl) ionic liquid, and a PB paste as the cathodic material. The resulting dual-chamber alcohol biobattery oxidizes ethanol to acetaldehyde during the discharge phase, followed by the conversion of acetaldehyde to ethanol in the charging period. Simultaneously, Berlin green (BG) is reduced to PB during discharge at the cathode and oxidized back to PB when the battery is charged. Xie et al. [14] reported the use of PB as the cathode material of a single-chamber membraneless microbial biobattery. In this biobattery the reduction of the PB film is driven by the oxidation of glucose catalyzed by the bacterial biofilm at the anode. Their biobattery reached net biomass energy recovery efficiencies of 18–33%.

Here, we propose the use of solid-state PB as the cathode material in enzymatic implantable devices. On this basis, a rechargeable glucose biobattery was fabricated with an aqueous electrolyte based on a PB thin-film cathode and glucose oxidase (GOx) enzymatic anode, both of which were immobilized on carbon paper substrates. To the best of our knowledge, this is the first study showing the use of solid-state PB thin-films in a rechargeable glucose enzymatic biobattery. The resulting membraneless biobattery offers several advantages for powering both implantable devices and portable sensors: (i) PB is a non-toxic and low-cost material with a simple and scalable synthesis from earth abundant elements, (ii) the use of a solid-state cathode eliminates the need for O_2 as the electron acceptor and is not associated with the energy loss due to the diffusion overpotential of dissolved O_2, (iii) hydrogen peroxide (H_2O_2) produced by undesirable side reactions at oxidase-based bioanodes can be reduced by the PB cathode, where Milton et al. [28,29] previously demonstrated that the parasitic production of H_2O_2 at the oxidase bioanodes by immobilized GOx negatively influence the performance of both laccase and bilirubin oxidase (BOx) biocathodes and the final power output of single-chamber EFCs, (iv) PB-based cathodes can be regenerated after reduction by being exposed to ambient air, and this process does not require the input of energy, and (v) the proposed fabrication technique of the PB thin-film modified with multi-walled carbon nanotubes (MWCNTs) can be implemented for producing
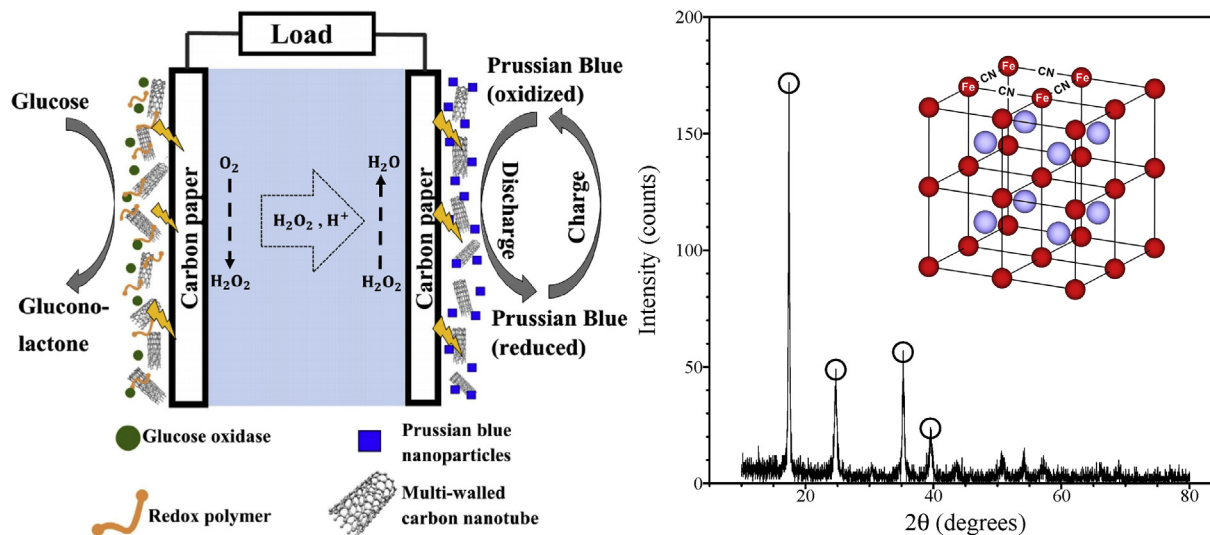

Fig. 1. (Left) Schematic of the glucose biobattery configuration. (Right) Powder X-ray diffraction (XRD) patterns of the as-prepared PB nanoparticles, with the crystal structure of PB being shown on the top right of the graph.

ultra-thin power units such as paper-based green batteries.

2. Experimental

2.1. Materials and chemicals

Glucose oxidase (GOx, from 'Aspergillus niger', EC 1.1.3.4, Type X-S), tetrabutylammonium bromide (TBAB), (6-Bromohexyl) ferrocene, and Nafion 5 wt% suspension were purchased from Sigma-Aldrich. Bilirubin oxidase (BOx from 'Myrothecium sp.', EC 1.3.3.5) was ordered from Amano enzyme (Japan). LPEI (MW 100,000) and ethylene glycol diglycidyl ether (EGDGE) were purchased from Polyscience Inc., Warrington, PA.

HCl (30%) was purchased from Macron Fine Chemicals™. Ferric chloride $FeCl_3$, and potassium ferricyanide $K_3[Fe(CN)_6]$ were obtained from Sigma-Aldrich. Hydrogen peroxide (30%), citric acid, sodium phosphate dibasic anhydrous, and dextrose (D-glucose) anhydrous were purchased from Fisher Scientific. Toray carbon paper 0.90" (non-wet proofed) was purchased from Fuel Cell Earth. Carboxyl-modified multi-walled carbon nanotubes (MWCNT) were obtained from www.cheaptubes.com. All chemicals were used as received without further purification.

Hexylferrocenyl-LPEI (Fc-C_6-LPEI) was synthesized following procedures reported in Refs. [30,31]. Briefly, 10 mL of acetonitrile was mixed with 300 mg of linear polyethylenimine. The solution was then refluxed under vigorous agitation for approximately 10 min. Afterwards, 2 mL of ethanol and 380 mg of (6-Bromohexyl) ferrocene were added to the mixture and refluxed overnight. Finally, the polymer extracted by removing the solvents from the mixture with the aid of diethyl ether. Synthesis of TBAB-modified Nafion was adopted from Refs. [32,33]. Anthracene-modified multi-walled carbon nanotubes (An-MWCNTs) were modified as described in Refs. [34–36].

Prussian Blue nanoparticles were synthesized by a chemical precipitation method, adopted from Refs. [14,37]. Briefly, 0.5 M $K_3[Fe(CN)_6]$ and 0.5 M $FeCl_3$ were added under vigorous agitation to water that had been adjusted to pH 2.0 using HCl. Afterwards, the solution was stirred overnight at 50 °C, allowing the evaporation of solvent. Finally, the precipitates were collected by centrifugation at 4000 rpm, and washed with excessive deionized (DI) water. This process was repeated several times until a clear separation between the chemical precipitates and the solvent was observed. The nanoparticles were then dried for 1 h at 100 °C. The as-prepared PB nanoparticles were evaluated with powder X-ray diffraction (XRD) to verify the formation of PB crystal. As shown by Fig. 1 (right), the pronounced peaks of the XRD graph at 2θ of 17.4, 25.6, 35.2, and 29.4 marked with circles are ascribed to the crystal structure of $Fe[Fe(CN)_6]_3 \cdot xH_2O$ [37,38].

2.2. Instrumentation

Electrochemical analysis was conducted utilizing a CHI 660E potentiostat (CH Instrument, USA). Electrode characterization and half-cell tests were conducted in a three-electrode setup where a saturated calomel electrode (SCE) and a platinum mesh (1 cm^2 projected surface area) were used as reference and counter electrodes, respectively. All the electrochemical tests were performed at room temperature (21 °C) and by using a 0.2 M citrate/phosphate buffer solution (pH 7.0) as the supporting electrolyte. Current and power densities were normalized with respect to the projected surface area of the anode. Battery cells were fabricated using a desktop 3D-printer (Formlabs Form 1+), with clear photopolymer resin.

2.3. Bioelectrode preparation

The GOx and BOx electrodes were prepared following the steps described in Refs. [28,39]. Briefly, for 3 cm^2 coating of GOx anodes, 140 μL of 10 mg mL^{-1} hexylferrocenyl-LPEI polymer in DI water was mixed with 60 μL of 10 mg mL^{-1} GOx solution in DI water. Then, 5.5 μL of EGDGE solution (10% v/v in DI water) was added to the mixture, followed by vortex mixing until homogenization. The solution was then spread on carbon paper electrodes, and left at room temperature to dry for 24 h. To coat 3 cm^2 of BOx cathodes, 1.5 mg of BOx was dissolved in 75 μL of 0.2 M citrate/phosphate buffer (pH 7.0). Then, 7.5 mg of An-MWCNTs was added to the solution, followed by consecutive steps of vortex mixing (1 min) and sonication (15 s), until the solution is homogenized. Afterwards, 25 μL of TBAB-modified Nafion was added to the mixture, followed by three steps of vortex mixing and sonication. The resulting slurry was then brush-coated on one side of a carbon paper substrate, and left under the positive air flow to dry for at least 4 h.

2.4. PB electrode preparation

To prepare 1 cm^2 of PB electrode, 6 mg of the PB nanoparticles was added to 100 μL of isopropyl alcohol and 30 μL of DI water with 14 MΩ cm resistivity. The solution was vortex mixed thoroughly until a dark blue color was observed. Afterwards, 2 mg of carboxylated MWCNT (referred to as MWCNT) was added to the mixture, followed by sonication for 30 min. Then, 5 μL of 5 wt% Nafion was added to the mixture, vortex mixed for 30 s, and sonicated for another half an hour to make sure a stable dispersion of nanoparticles was achieved. The slurry was then brush-coated layer-by-layer on one side of the carbon paper. In this process, after brushing one layer, the electrode was immediately exposed for a few seconds to light illumination which helps to evaporate the solvent. The as-prepared electrodes were then placed in an oven overnight at 100 °C which was found to stabilize the PB/MWCNT composite. In this study, we refer to the PB/MWCNT composite electrodes as PB thin-film electrodes. Before performing the tests, the bare surface of the carbon paper was coated with wax to exclude it from the electrochemically active area of the cathode.

3. Results and discussion

In the first step, the immobilization of the enzymes on the carbon paper substrate was investigated via cyclic voltammetric (CV) studies. For the GOx bioanode, it was determined that a minor modification of the untreated carbon paper with MWCNT enhances the conductive sites for electron transfer and slightly improves the onset potential for glucose oxidation (Fig. 2a). The open circuit voltage (OCV) test of the anodic half-cell in buffer containing 0.1 M glucose demonstrates that the onset potential decreases from approximately 0.1 V to −0.08 V (vs. SCE). This improvement enhances the OCV of the biobattery, and is mainly attributed to the increased active surface area for chemical adsorption and overcoming diffusion limitations. Moreover, the catalytic current is improved by ca. 24% due to the enhancement in the surface conductivity by MWCNT. Fig. 2b represents the CVs of the as-prepared O_2-reducing BOx cathode. As seen, the injection of O_2 introduces a significant catalytic current, showing the successful immobilization of BOx in an An-MWCNT/TBAB-modified Nafion on carbon paper.

In the next step, the power output of the glucose biobattery with the setup shown in Fig. 1 was tested and evaluated against a conventional EFC in which the PB cathode was replaced by the BOx cathode (O_2-reducing) with the electrolyte being saturated by O_2. The power curves are obtained by sweeping the voltage between
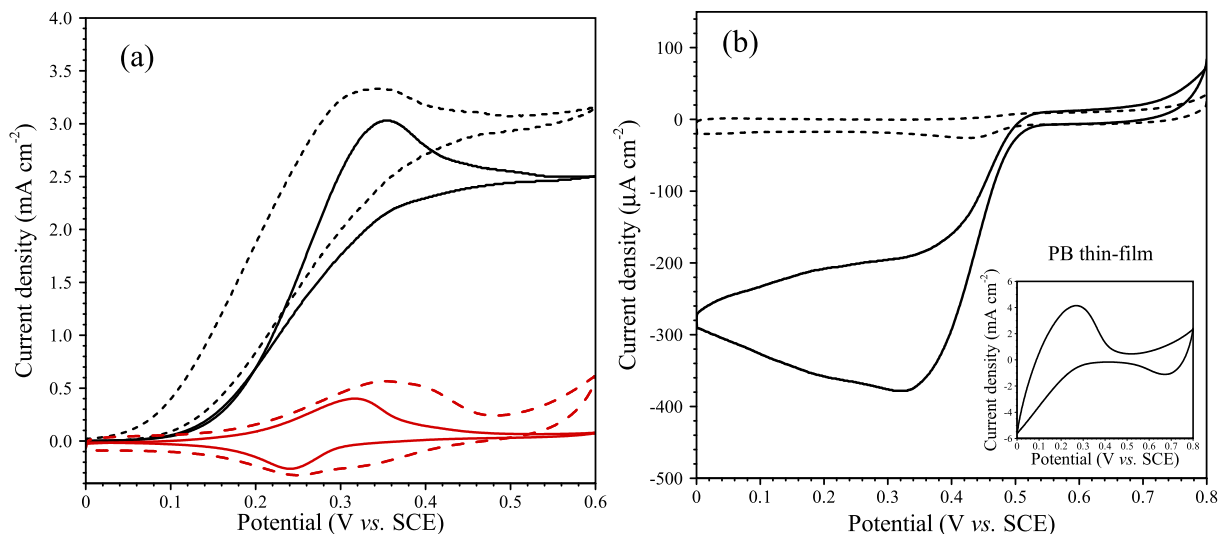
Fig. 2. Representative cyclic voltammograms of the as-prepared enzymatic electrodes at a scan rate of 1mV s^{-1}. (a) GOx/Fc-C$_6$-LPEI (——) and GOx/Fc-C$_6$-LPEI/MWCNT anode (– – ·) in the presence (black) and the absence (red) of 0.1 M glucose. (b) BOx/An-MWCNT/TBAB-modified Nafion cathode in the presence (——) and absence (– – ·)of O$_2$. (b, inset) PB-thin film in the absence of at a scan rate of 1 mV s^{-1}O$_2$. (For interpretation of the references to colour in this figure legend, the reader is referred to the web version of this article.)

the OCV of the cell to 0 at a scan rate of 1mV s^{-1}. Before the linear polarization tests, the OCV of the cell setup was measured for at least 500 s, until a stable curve is obtained. The OCV of the glucose|PB biobattery was *ca.* 0.45 V while the OCV of the glucose|O$_2$ EFC was *ca.* 0.6 V, which is ascribed to the larger theoretical half-cell potential of the O$_2$-reducing cathode. As shown by Fig. 3a, the use of the solid-state PB thin-film cathode yielded an increased power output (by *ca.* 37%) and short-circuit current density (by *ca.* 180%) to 44 μW cm^{-2} and 0.9 mA cm^{-2}, respectively, compared to an EFC equipped with an O$_2$-reducing cathode. Factors contributing to this performance are mainly associated with the transition from the enzymatic reduction of O$_2$ to the solid-state electrode in the cathode side as defined below.

First, the use of a solid-state electrode overcomes the diffusion overpotential (especially in hydrostatic/quiescent electrolytes). Secondly, achievable concentrations of dissolved O$_2$ in the

electrolyte is limited by temperature and pressure, requiring the input of energy. Third, the O$_2$ dissolved in the bulk electrolyte (for the cathode) may in fact interfere in the oxidation of glucose at the anode (in membraneless configurations). For instance, it is well understood that GOx reduces O$_2$ to H$_2$O$_2$ by the chemical reaction below, in which flavin adenine dinucleotide (FAD) is the redox co-factor of the GOx [28]:

$$GOx(FADH_2) + O_2 \rightarrow GOx(FAD) + H_2O_2 \qquad (1)$$
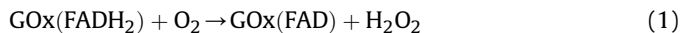
The production of H$_2$O$_2$ may reduce enzymatic activity of both the cathode and anode, which is a key factor of reduced power output after long operational cycles [28]. Unfortunately, utilizing an O$_2$-reducing cathode has been the primary choice for most implantable devices, since assembling an air-breathing gas diffusion layer for *in vivo* applications is problematic, especially for
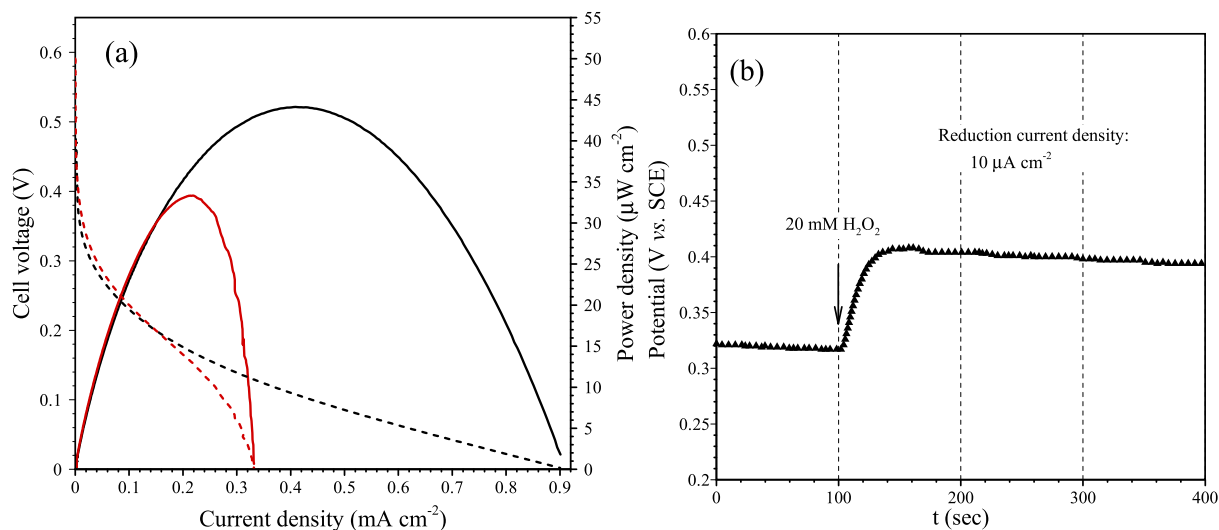

Fig. 3. (a) Power curves (solid lines) and linear polarization graphs (dashed lines) of the glucose|PB (black), and glucose|O$_2$ (red) in the buffer solution containing 0.1 M glucose for both cases, and saturated by O$_2$ for the latter case. The linear polarization graphs were obtained by sweeping the voltage between the OCV of the cell to 0 at a scan rate of 1 mV s^{-1}. The OCVs were measured by maintaining the cell at zero current until a stable voltage is observed. (b) Chronopotentiometry study of the PB thin-film cathode in the buffer solution being injected by H$_2$O$_2$ at t = 100 s. (For interpretation of the references to colour in this figure legend, the reader is referred to the web version of this article.)

membraneless and miniaturized designs. On the other hand, the solid-state PB cathode eliminates the need for O_2, and H_2O_2 produced by the GOx bioanode can be reduced to water in neutral media by the following reaction [37,40]:

$$H_2O_2 + 2H^+ + 2e^- \rightarrow 2H_2O \tag{2}$$

In order to see if the PB thin-film cathode can reduce small amounts of H_2O_2 in the bulk electrolyte during operation, the cathodic half-cell was evaluated by chronopotentiometry, in which a constant reducing current is applied to the PB electrode. As shown by Fig. 3b, a sudden increase in the cathodic half-cell potential is observed after the addition of 20 mM of H_2O_2 at t = 100 s. This increase in the voltage shows the appropriate H_2O_2 sensitivity of the as-prepared PB thin-film electrode, and is attributed to the reduction potential of H_2O_2 [1.77 vs. standard hydrogen electrode (SHE)].

Many studies have shown that the cyclic voltammetric behavior of PB involves two redox states namely Berlin Green (BG) (or Prussian Yellow in some cases) and Prussian White (PW). BG is the fully oxidized state of PB occurring at high potentials, while PW is the fully reduced and colorless state of PB at low potentials. Here we intend to show that the as-prepared PB thin-film electrodes

may be regenerated by ambient air (charging phase) after being partially reduced to PW in the biobattery (discharging phase). Note that, unlike refs. [14,27], we do not electrochemically reduce (before the discharging period) or oxidize (during charging period) the as-prepared PB thin-film electrodes, which is beneficial to maintain the energy balance. As a proof-of-concept, a battery cell was 3D-printed and filled with buffer solution containing 0.1 M glucose, with the electrodes being located 2 cm apart. Note that since the electrolyte is not purged with O_2, we expect H_2O_2 formation by the GOx bioanode remains at low concentrations, as demonstrated in Fig. 3b; thus, its reduction by the PB thin-film cathode is not the main source of overall power production. The cell is then maintained at a constant current density of 10 μA cm^{-2} for 20 cycles. In each cycle, after 5 min of discharge, the PB thin-film cathode was removed from the cell, exposed to ambient air for 5 min and installed back into the battery for another discharge period of the same time. Fig. 4a represents the cycling data of the glucose biobattery. First of all, in the very beginning of each discharge phase, the cell voltage drops by nearly 0.7 V. However, this reduction is mainly attributed to the voltage loss in the anodic half-cell, as shown by the chronopotentiometry study of the GOx electrode in Fig. 4b. The average cell voltage during the discharge
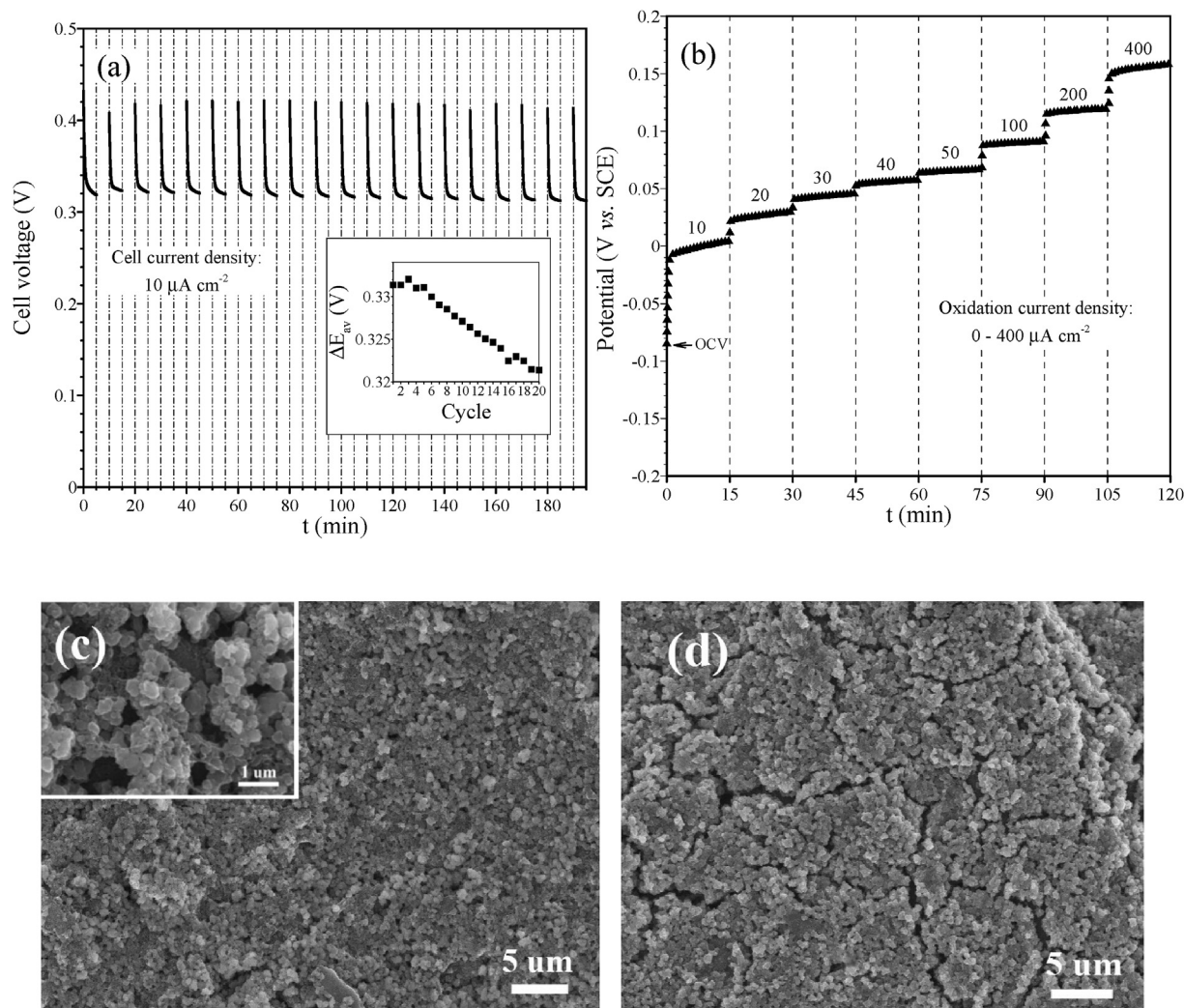

Fig. 4. (a) Cycling performance of the glucose biobattery, and the average cell voltage being plotted versus the cycle number. (b) Chronopotentiometry study of the anodic half-cell. Scanning electron microscopy (SEM) images of the PB thin-film on carbon paper substrate before (c) and after (d) the cycling study. All electrochemical tests were performed in buffer solution containing 0.1 M glucose.

phase was then calculated and plotted *versus* the cycle number in Fig. 4a. As seen, the average cell voltage drops by nearly 3% after 20 cycles which is mainly attributed to the loss of capacity of the PB, and deterioration of the thin-film due to continual removal, drying and reintroduction to the aqueous electrolyte. The latter was concluded due to the cracks that appeared in the PB thin-film after operation, as shown by comparing the SEM images in Fig. 4c and d.

If the biobattery is to be recharged by dissolving O_2 in the bulk electrolyte, the amount of H_2O_2 produced by the GOx bioanode can end up being higher than the dissolved O_2 concentration. As long as the sensitivity of the PB thin-film cathode towards reducing H_2O_2 is retained, this is expected to benefit the biobattery during off cycles, as the reduction of H_2O_2 by the PB thin-film cathode can recover some energy losses. However, dissolving O_2 requires the input of energy, and we insist on minimizing the overall energy input to exploit power from glucose. Therefore, unless techniques (such as designing a flow-through device) are devised to introduce O_2-containing electrolyte to charge the biobattery without spending energy, the biobattery would mostly benefit from being recharged by ambient air.

With respect to *in vivo* application, we do not envisage utilizing the proposed biobattery in areas where oxygen availability is extremely low. Even if this is the case, the proposed biobattery will turn into a primary cell with the performance characteristics shown in Fig. 3a, which demonstrates noticeable improvement compared to the conventional EFCs and is potentially applicable for *in vivo* power generation. In the presence of ample oxygen concentrations required for running a conventional EFC, the use of the PB cathode is still preferable due its ability to reduce the H_2O_2 formed by the anodic side reaction, enabling the enzymatic biobattery to effectively operate in a membraneless configuration.

4. Conclusion

A membraneless rechargeable glucose biobattery combining a GOx bioanode and a PB thin-film cathode was presented. The use of PB diminishes problems associated with the formation of peroxide as a function of GOx side reactions taking place at the bioanode, as the PB is known to be highly electroactive towards reducing H_2O_2. In this regard, the role of PB is significant especially in membraneless designs where H_2O_2 can diffuse to the cathodic side of the EFCs and destabilize the performance of enzyme-based cathodes. Moreover, solid-state PB cathodes may replace cathodes that deplete dissolved O_2 in the electrolyte, overcoming diffusion overpotentials and improving the overall performance. PB has also been recognized by its two redox pairs (PW/PB at low potentials and PB/BG at high potentials), allowing it to function as a rechargeable cathode material.

All these features along with the biocompatibility of the materials utilized in this category of glucose biobatteries enable its use as an energy harvester in *in vivo* environments where soluble electron donors (and not the electron acceptors) are easily exploitable. Specifically, this biobattery is potentially useful in an intravenous environment where the bioelectrodes are embedded into the walls of blood vessels and take advantage of the enhanced mass transfer afforded by the blood circulation. However, to apply this concept to biological samples, the bioelectrodes need to be engineered on the nano-scale to reduce the size of the device while maintaining or even increasing the reaction sites, sensitivity, and stability of the glucose oxidizing anode and PB reducing cathode.

References

[1] M. Rasmussen, S. Abdellaoui, S.D. Minteer, Biosens. Bioelectron. 76 (2016) 91–102.
[2] M.T. Meredith, S.D. Minteer, Annu. Rev. Anal. Chem. 5 (2012) 157–179.
[3] A.A. Yazdi, L. D'Angelo, N. Omer, G. Windiasti, X. Lu, J. Xu, Biosens. Bioelectron. 85 (2016) 536–552.
[4] D. Pankratov, R. Sundberg, J. Sotres, I. Maximov, M. Graczyk, D.B. Suyatin, E. González-Arribas, A. Lipkin, L. Montelius, S. Shleev, J. Power Sources 294 (2015) 501–506.
[5] R.D. Milton, K. Lim, D.P. Hickey, S.D. Minteer, Bioelectrochemistry 106 (2015) 56–63.
[6] L. Zhang, L. Chen, X. Zhou, Z. Liu, Adv. Energy Mater. 5 (2015).
[7] Y. Ogawa, Y. Takai, Y. Kato, H. Kai, T. Miyake, M. Nishizawa, Biosens. Bioelectron. 74 (2015) 947–952.
[8] S. Aquino Neto, R.D. Milton, D.P. Hickey, A.R. De Andrade, S.D. Minteer, J. Power Sources 324 (2016) 208–214.
[9] K. Monsalve, I. Mazurenko, N. Lalaoui, A. Le Goff, M. Holzinger, P. Infossi, S. Nitsche, J. Lojou, M. Giudici-Orticoni, S. Cosnier, Electrochem. Commun. 60 (2015) 216–220.
[10] M.J. González-Guerrero, J.P. Esquivel, D. Sánchez-Molas, P. Godignon, F.X. Muñoz, F.J. Del Campo, F. Giroud, S.D. Minteer, N. Sabaté, Lab a Chip 13 (2013) 2972–2979.
[11] C. Fischer, A. Fraiwan, S. Choi, Biosens. Bioelectron. 79 (2016) 193–197.
[12] S. Calabrese Barton, J. Gallaway, P. Atanassov, Chem. Rev. 104 (2004) 4867–4886.
[13] T. Miyake, K. Haneda, N. Nagai, Y. Yatagawa, H. Onami, S. Yoshino, T. Abe, M. Nishizawa, Energy & Environ. Sci. 4 (2011) 5008–5012.
[14] X. Xie, M. Ye, C. Liu, P.-C. Hsu, C.S. Criddle, Y. Cui, Energy & Environ. Sci. 8 (2015) 546–551.
[15] P. Padigi, J. Thiebes, M. Swan, G. Goncher, D. Evans, R. Solanki, Electrochim. Acta 166 (2015) 32–39.
[16] Y. You, X. Yu, Y. Yin, K.-W. Nam, Y.-G. Guo, Nano Res. 8 (2015) 117–128.
[17] H.-W. Lee, R.Y. Wang, M. Pasta, S.W. Lee, N. Liu, Y. Cui, Nat. Commun. 5 (2014).
[18] H. Lee, Y.-I. Kim, J.-K. Park, J.W. Choi, Chem. Commun. 48 (2012) 8416–8418.
[19] S. Liu, G. Pan, G. Li, X. Gao, J. Mater. Chem. A 3 (2015) 959–962.
[20] R. Trócoli, F. La Mantia, ChemSusChem 8 (2015) 481–485.
[21] Z. Jia, B. Wang, Y. Wang, Mater. Chem. Phys. 149 (2015) 601–606.
[22] Z. Liu, G. Pulletikurthi, F. Endres, ACS Appl. Mater. interfaces 8 (2016) 12158–12164.
[23] A.A. Karyakin, E.A. Puganova, I.A. Bolshakov, E.E. Karyakina, Angew. Chem. Int. Ed. 46 (2007) 7678–7680.
[24] A.A. Karyakin, O.V. Gitelmacher, E.E. Karyakina, Anal. Chem. 67 (1995) 2419–2423.
[25] A.N. Sekretaryova, V. Beni, M. Eriksson, A.A. Karyakin, A.P. Turner, M.Y. Vagin, Anal. Chem. 86 (2014) 9540–9547.
[26] Y. Yu, M. Xu, S. Dong, Chem. Commun. 52 (2016) 6716–6719.
[27] P.K. Addo, R.L. Arechederra, S.D. Minteer, J. Power Sources 196 (2011) 3448–3451.
[28] R.D. Milton, F. Giroud, A.E. Thumser, S.D. Minteer, R.C. Slade, Phys. Chem. Chem. Phys. 15 (2013) 19371–19379.
[29] R.D. Milton, F. Giroud, A.E. Thumser, S.D. Minteer, R.C. Slade, Electrochim. Acta 140 (2014) 59–64.
[30] S.A. Merchant, T.O. Tran, M.T. Meredith, T.C. Cline, D.T. Glatzhofer, D.W. Schmidtke, Langmuir 25 (2009) 7736–7742.
[31] S.A. Merchant, M.T. Meredith, T.O. Tran, D.B. Brunski, M.B. Johnson, D.T. Glatzhofer, D.W. Schmidtke, J. Phys. Chem. C 114 (2010) 11627–11634.
[32] T.J. Thomas, K.E. Ponnusamy, N.M. Chang, K. Galmore, S.D. Minteer, J. Membr. Sci. 213 (2003) 55–66.
[33] N.L. Akers, C.M. Moore, S.D. Minteer, Electrochim. Acta 50 (2005) 2521–2525.
[34] A. Dawn, T. Shiraki, S. Haraguchi, H. Sato, K. Sada, S. Shinkai, Chem. A Eur. J. 16 (2010) 3676–3689.
[35] M. Minson, M.T. Meredith, A. Shrier, F. Giroud, D. Hickey, D.T. Glatzhofer, S.D. Minteer, J. Electrochem. Soc. 159 (2012) G166–G170.
[36] R.D. Milton, F. Giroud, A.E. Thumser, S.D. Minteer, R.C. Slade, Chem. Commun. 50 (2014) 94–96.
[37] S.A.M. Shaegh, N.-T. Nguyen, S.M.M. Ehteshami, S.H. Chan, Energy & Environ. Sci. 5 (2012) 8225–8228.
[38] G. Selvarani, S. Prashant, A. Sahu, P. Sridhar, S. Pitchumani, A. Shukla, J. Power Sources 178 (2008) 86–91.
[39] M.T. Meredith, D.-Y. Kao, D. Hickey, D.W. Schmidtke, D.T. Glatzhofer, J. Electrochem. Soc. 158 (2011) B166–B174.
[40] A.A. Karyakin, Electroanalysis 13 (2001) 813–819.